Applied Catalysis A: General xxx (2013) xxx–xxx

Contents lists available at ScienceDirect

Applied Catalysis A: General

journal homepage: www.elsevier.com/locate/apcata

Effect of the size and distribution of supported Ru nanoparticles on their activity in ammonia synthesis under mild reaction conditions

Camila Fernández[a,*], Capucine Sassoye[b], Damien P. Debecker[a], Clément Sanchez[b], Patricio Ruiz[a]

[a] Institute of Condensed Matter and Nanosciences – IMCN, Division "Molecules, Solids and Reactivity-MOST", Université catholique de Louvain, Croix du Sud 2, 1348 Louvain-la-Neuve, Belgium
[b] Laboratoire de Chimie de la Matière Condensée de Paris, Collège de France, Paris 75005, France

ARTICLE INFO

Article history:
Received 13 April 2013
Received in revised form
16 September 2013
Accepted 20 September 2013
Available online xxx

Keywords:
Low-temperature ammonia synthesis
Ru supported catalyst
Nanoparticle
Size distribution
Catalytic cooperation

ABSTRACT

Ru/γ-Al_2O_3 catalysts were prepared using three different methods: wet impregnation, colloidal method and microemulsion. Ru-supported nanoparticles with different average sizes and distribution of sizes were obtained. The catalysts were tested in ammonia synthesis under mild reaction conditions, namely low temperature (100 °C) and low pressure (4 bar), and characterized by N_2 adsorption, XRD, XPS, TEM and TPR techniques. The results indicate that a good catalytic performance can be achieved by Ru supported nanoparticles fulfilling two requirements: (i) a relatively high average size (despite the usual assertion that only small particles are required) and (ii) a broad distribution of sizes that ensures the presence of both small particles, containing highly active sites, and large nanoparticles, which are shown to promote the reaction on small particles. This promotion results from a cooperative effect between small and large nanoparticles in good contact, which also allows keeping a highly reduced surface of ruthenium.

It is proposed that, under mild reaction conditions, large Ru nanoparticles promote the ammonia synthesis reaction by allowing a more effective activation and transfer of hydrogen atoms, able to hydrogenate strongly adsorbed nitrogen atoms, and thus to release active sites for the activation of N_2.

1. Introduction

Ammonia synthesis is one of the highest energy consumer processes in the chemical industry. This exothermic reversible reaction is strongly limited by the thermodynamic equilibrium, so the industrial operating conditions have been set to high temperatures (300–500 °C) and high pressures (100–200 bar). The synthesis of highly active catalysts and the development of new concepts in ammonia synthesis at low temperature open interesting possibilities for improving existing technologies and for designing new processes of low energy consumption [1,2]. The use of Ru-based nanocatalysts has been shown to be a key factor to perform this reaction under mild conditions [3–8]. It has been claimed that metal-supported nanoparticles present high catalytic performances, not exclusively due to the high surface area, but also because of the special properties arising from the nano-size dimension, which are expected to change the electronic structure of the metal, thus leading to unusual catalytic activities [9,10].

The N_2 dissociative adsorption is the rate-determining step in ammonia synthesis. Density functional calculations (DFT) have shown that there is a linear relationship (Brønsted–Evans–Polanyi type) between the activation barrier of N_2 dissociation and the energy of N_2 dissociative chemisorption [11,12]. According to this relationship, a reduction in the activation barrier of N_2 dissociation may lead to a surface blocking by adsorbed nitrogen atoms. DFT calculations [13–15] indicate that the most active sites for N_2 dissociative adsorption are the B_5-type sites, exposing a three-fold hollow site close together with a bridge site. These sites ensure that the two nitrogen atoms are not bonded to the same Ru atom during the dissociation, thus leading to a significant decrease in activation energy without a similar increase in the adsorption energy of nitrogen atoms. Dahl et al. [13,14] proposed that the N_2 dissociation on the Ru(0 0 0 1) single-crystal plane only occurs at mono atomic steps, whose reactivity is significantly higher than the activity of atoms on terraces. It has been suggested that the catalytic performance of Ru surfaces can be determined by the concentration of B_5-type sites. Jacobsen et al. [15] have shown that the probability of forming B_5 sites is maximum for sizes of 1.8–2.5 nm, and it decreases for larger particles. They obtained very low TOFs (at 475 °C and 50 bar in 3:1 H_2/N_2) for the Ru/$MgAl_2O_4$ catalyst having Ru crystals smaller than 1 nm, which are expected to contain a low number of B_5 sites. Recently, Lin et al. [16] showed that

* Corresponding author. Tel.: +32 10 47 35 91.
E-mail addresses: camila.fernandez@uclouvain.be (C. Fernández), ruiz@cata.ucl.ac.be (P. Ruiz).

0926-860X/$ – see front matter © 2013 Elsevier B.V. All rights reserved.
http://dx.doi.org/10.1016/j.apcata.2013.09.039

Sm-promoted Ru nanoparticles supported on γ-Al_2O_3 with an average size of 2.1 nm are the most active under conditions of high temperature (200–500 °C) and pressure (100 bar). Additionally to the size effect of the Ru nanoparticles, changes in the active sites properties were proposed to explain catalytic results.

The effect of the Ru particle size on the catalytic performance has been also studied in the presence of alkali promoters, which are known to affect the electronic properties of the active sites and even modify the specific surface. The results reported show that the catalytic activity increases with the size of Ru crystallites. For Ba-promoted Ru/C catalysts, Kowalczyk et al. [17] found that the TOF value (at 400 °C and 60 bar in 3:1 H_2/N_2, 8% NH_3) increases with the Ru particle size, reaching a constant value for particles larger than 3 nm. Rarog-Pilecka et al. [18] obtained the same trend for Cs-promoted catalysts, at similar conditions (400 °C and 63 bar, in 3:1 H_2/N_2, 8.5% NH_3). According to Liang et al. [19], the TOF value (at 400 °C and 30 bar in 3:1 H_2/N_2) increases with the Ru particle size ranging from 2 to 10 nm, for K and Ba-promoted Ru/C catalysts.

However, all these results have been obtained for the reaction at high temperatures (>400 °C) and pressures (>30 bar). Under mild reaction conditions, it is expected that other features in the surface configuration of Ru nanocatalyst will affect its catalytic activity.

The aim of this work is to study the catalytic performance of Ru-supported nanocatalysts in ammonia synthesis under mild reaction conditions, and to determine the effect of the catalyst surface configuration (distribution of particles on the support, particle sizes and distribution of sizes) on the activity. Until now the literature is poor in studies addressing these issues for the ammonia synthesis reaction performed at truly mild conditions (<200 °C).

For this purpose we have synthesized catalytic Ru-supported nanoparticles with different tailored-size distributions, by (i) the traditional wet impregnation of the support with the Ru precursor and (ii) the deposition on the support of a suspension containing RuO_2 nanoparticles already formed by a colloidal method [20] or microemulsion [21], which is known to allow the synthesis of small particles with a narrow size distribution [22,23]. The catalysts were used to produce ammonia from nitrogen and hydrogen, at low temperature (100 °C) and low pressure (4 bar). In order to study the activity of the Ru nanoparticles as a function of their size, distribution of sizes and Ru oxidation state, the catalysts were analyzed by X-ray diffraction, X-ray photoelectron spectroscopy and transmission electronic microscopy. The results obtained in this work not only allow a better understanding of the catalytic performance of Ru-supported nanoparticles in ammonia synthesis, but could also provide insights into the catalytic performance of other noble metal in reactions operating at mild conditions.

2. Experimental

2.1. Synthesis of catalysts

Samples denoted as 'calcined' correspond to 450 °C calcined fresh catalysts, while samples denoted as 'tested' correspond to catalysts obtained after the catalytic test, which includes the reduction pretreatment and the subsequent ammonia synthesis reaction.

2.1.1. Wet impregnation (WI)

Catalysts were prepared by wet impregnation of γ-Al_2O_3 (Alfa Aesar, S_{BET} = 73 m^2/g). The powdered support was dipped into an aqueous solution of ruthenium (III) chloride hydrate (Alfa Aesar, 99.99%), in the amount required to obtain a theoretically 2, 3 and 7 wt.% of Ru. After stirring for 2 h at room temperature, the solvent was evaporated under reduced pressure, in a rotavapor at 35 °C. The resulting solid was dried at 110 °C overnight and later calcined in air at 450 °C for 4 h. The catalysts are denoted as Ru*X*/Al-WI (*X*: 2, 3 or 7 wt.%).

2.1.2. Colloidal method (COLL)

Catalysts were prepared by depositing on γ-Al_2O_3 a colloidal suspension of RuO_2 nanoparticles. The colloidal suspension was synthesized via hydrolysis, by using H_2O_2 as oxidizing agent and surface etchant to achieve the particle size control [20]. An aqueous solution of H_2O_2 (Acros Organics, 35 wt.%) was slowly added into a solution of $RuCl_3{\cdot}3H_2O$ (Alfa Aesar, 99.99%), under magnetic stirring. The suspension was placed in an oven at 95 °C for 2 hours and after cooling down to room temperature, the powdered support was added under vigorous agitation. The catalyst was recovered via evaporation of the solvent in rotavapor under reduced pressure at 50 °C, and then it was calcined in air at 450 °C for 16 h. The catalysts are denoted as Ru*X*/Al-COLL (*X*: 3 or 7 wt.%).

2.1.3. Microemulsion method (MIC)

Catalysts were synthesized via the water in oil microemulsion method [21–23]. Oil phases containing different surfactants, tetraethylene glycol dodecyl ether (Brij30, Sigma–Aldrich, 99.9%), sodium bis(2-ethylhexyl)sulfosuccinate (AOT, Sigma–Aldrich, 99.9%) or hexadecyltrimethylammonium bromide (CTAB, Alfa Aesar, 99.9%) and organic solvents (n-heptane, 1-butanol or cyclohexane, Fluka, 99.9%) were used. Hydrazine hydrate (Fluka, 80%) was used as the reducing agent. The molar ratios of surfactant-to-Ru and water-to-surfactant were maintained at 40:1 and 9:1, respectively. A solution of $RuCl_3{\cdot}3H_2O$ in distilled water was added, under magnetic stirring, into an oil phase containing the appropriate amount of surfactant in 50 ml of organic solvent. Always under stirring, the microemulsion was heated up to 60 °C in a thermostated oil bath and then the γ-Al_2O_3 support was added. After 30 min, hydrazine was injected in an amount corresponding to a hydrazine-to-Ru molar ratio of 9:1. After 30 min of reduction, the solution was washed with acetone (99%, VWR) and distilled water. The resulting solid was dried at 110 °C overnight and calcined in air at 450 °C for 4 h. The catalysts are denoted as Ru3/Al-MIC X/Y, where X corresponds to the surfactant and Y to the organic solvent.

2.1.4. Mechanical mixtures

Mechanical mixtures of Ru3/Al-WI and Ru7/Al-WI, in different percentages (25, 50 and 75 wt.%), were obtained by dispersing both catalysts in n-pentane (Merck, >98%) under vigorous agitation assisted by ultrasonic dispersion. The n-pentane was evaporated under agitation at 25 °C and the recovered solid was dried at 110 °C overnight. After drying, the mixtures were not calcined. The single Ru3/Al-WI and Ru7/Al-WI catalysts were subjected to exactly the same treatment as the mixtures. Mixtures are denoted as 75Ru3/Al-WI + 25Ru7/Al-WI, 50Ru3/Al-WI + 50Ru7/Al-WI, 25Ru3/Al-WI + 75Ru7/Al-WI, where the numbers preceding each catalytic component (Ru3/Al-WI and Ru7/Al-WI) indicate the respective weight percentages in the mixture.

2.2. Catalytic activity measurements

Catalytic tests were carried out in a metallic fixed-bed tubular (i.d. 8 mm) reactor equipped with a frit to hold the catalyst and a K-type thermocouple to measure and control the temperature of the catalytic bed. The catalyst (400 mg) previously sieved to a particle size range of 100–315 μm was reduced in pure H_2 (Praxair, 4.8) at 200 °C during 2 h (heating rate of 10 °C/min). Isothermal experiments were performed in a flowing mixture (40 ml/min) of N_2/H_2 (1/3 vol.%), at 100 °C, 4 bar and a space velocity of 6000 ml/h/gcat. The effluents were analyzed online by using a gas chromatograph equipped with two thermal conductivity detectors. The sequence

of analyses was performed in periods of 15 min, allowing the quantification of NH_3, H_2 and N_2.

The specific reaction rate r, considering a tubular packed bed reactor is given by

$$r = \frac{dX_A}{d(W/F_A)} \quad (1)$$

where X_A and F_A correspond to the conversion and the molar flow of reactive A, and W is the catalyst mass. The reactor was operated at differential conditions ($X_A < 15\%$) at constant temperature. The rate of ammonia formation has been calculated as:

$$r = \frac{F_{N_2,i} X_{N_2}}{W} \quad (2)$$

For the ammonia synthesis, the rate of the backward reaction becomes considerable as the temperature increases. Therefore, the forward reaction rates were obtained by correcting the measured rates r_n (net reaction rates) with the approach to the equilibrium factor η:

$$r_{\text{forward}} = \frac{r_n}{1-\eta} \quad (3)$$

The η factor corresponds to the $r_{\text{backward}}/r_{\text{forward}}$ ratio and was calculated from the partial pressures (P_i) of reactants and products at the reactor exit, and the equilibrium constant (K_{eq}) of ammonia synthesis obtained by the software HSC Chemistry 4.0 [25]

$$\eta = \frac{P_{NH_3}^2}{P_{N_2} P_{H_2}^3} \cdot \frac{1}{K_{\text{eq}}} \quad (4)$$

The turnover frequency (TOF) values have been calculated as:

$$\text{TOF} = \frac{r_{\text{forward}}}{D} \cdot \frac{M}{L} \quad (5)$$

where M and L corresponds to the atomic mass of Ru and its loading (wt.%) in the catalyst. D is the dispersion of ruthenium, meaning the fraction of Ru surface atoms relative to the total Ru atoms present in the catalyst.

2.3. Physicochemical characterization

N_2 (Praxair, 5.0) adsorption and desorption isotherms of the samples were recorded at 77 K (temperature of liquid N_2) using a Micromeritics Tristar 3000 apparatus. Samples were previously degassed overnight at 150 °C and 0.15 mbar. The specific surface area was calculated according to the BET method.

Transmission electron microscopy (TEM) images were obtained with a FEI Tecnai 120 Twin microscope, operating at 120 kV and equipped with a Gatan Orius CCD numeric camera. The samples were prepared by ultrasonic dispersion of the powders in ethanol and a droplet of the dispersion was then placed onto a carbon-coated copper grid. Some samples were selected for a high-resolution analysis (HR-TEM) using a JEOL JEM 2010 microscope, operating at 200 kV and equipped with a Gatan camera. In this case, the samples were dispersed in water and deposited over commercial holey carbon-coated grids (200 mesh).

Frequency histograms of Ru nanoparticle sizes, mean size and standard deviation have been estimated with measured diameter from more than 100 particles on each sample. In order to fully appreciate the distribution of surface ruthenium atoms, the number of Ru particles in each range (from 1 to 12 nm, with 1 nm steep) from the previous histogram has been multiplied by the calculated surface of the particles (considered spherical), and then normalized.

X-ray diffraction (XRD) spectra were recorded with a Bruker D8 X-ray diffractometer, operating in the reflection mode with a Cu Kα radiation (λ = 1.5406 Å and 1.5444 Å), at 40 kV and 40 mA. The data were collected in the 20–50° range (2θ) with steps of 0.02°.

For the temperature programmed reduction (TPR) analysis, 200 g of catalyst (particle size range of 100–315 μm) were placed into a quartz U tube and subjected to a 10% H_2/He (Praxair) flow of 100 ml/min, while increasing the temperature up to 300 °C at a rate of 5 °C/min. The water formation was followed by mass spectroscopy.

X-ray photoelectron spectra were obtained for calcined and tested samples with a SIS-X-probe (SSX-100/206) spectrometer equipped with a monochromatized microfocused Al Kα X-ray source, operating at 10 kV and 12 mA. After outgassing under vacuum (10^{-5} Torr) overnight, the samples were placed in the analysis chamber where the residual pressure was of about 10^{-7} Torr. The charging effects, was adjusted using a flood gun energy at 8 eV and a fine-meshed nickel grid placed 3 mm above the sample surface. The pass energy was 150 eV and the spot size was 1000 μm, leading to an energy resolution of 1.6 eV. The angle between the normal to the sample surface and the direction of electron collection was 55°. The binding energy scale of the spectrometer was calibrated with respect to the Au $4f_{7/2}$ peak of gold fixed at 83.98 eV and the binding energies of O 1s, Al 2p, and Ru 3d were referenced to the C-(C,H) component of the C 1s band fixed at 284.8 eV. In order to obtain the surface atomic concentrations, the relative areas of the corresponding peaks were normalized by using sensitivity factors based on the Scofield cross-sections. The peak decomposition was performed using the CasaXPS program (Casa Software, UK), assuming a 85/15 Gaussian/Lorentzian product function and a Shirley non-linear sigmoid-type baseline.

The size of supported Ru particles was estimated from a model proposed by Kerkhof et al. [24], which considers catalysts consisting on cubic metallic crystallites of size (c) deposited over sheets of support. The thickness (t) of these sheets can be obtained from the density (ρ) and the surface area of the support, in this case:

$$r = \frac{2}{\rho_{Al_2O_3} S_{\text{BET,Al}}} \quad (6)$$

According to this model, the theoretical XPS $(Ru/Al)_m$ atomic ratio expected for a monolayer dispersion of ruthenium on alumina is given by

$$\left(\frac{Ru}{Al}\right)_m = \left(\frac{Ru}{Al}\right)_b \cdot \frac{D(\varepsilon_{Ru})}{D(\varepsilon_{Al})} \cdot \frac{\sigma_{Ru}}{\sigma_{Al}} \cdot \frac{1}{2} \left(\frac{t}{\lambda_{Al-Al}}\right) \cdot \frac{1+e^{-t/\lambda_{Ru-Al}}}{1-e^{-t/\lambda_{Ru-Al}}} \quad (7)$$

where $(Ru/Al)_b$ is the bulk atomic ratio calculated from the theoretical Ru content. D functions of the electron kinetic energies (ε) correspond to the spectrometer efficiencies and can be approximated as $1/\varepsilon$ [26]. σ_{Ru} and σ_{Al} are the relative photoelectron cross sections provided by Scofield [27]. λ_{Ru-Al} and λ_{Al-Al} correspond to the escape depths of Ru $3d_{3/2}$ and Al $2p_{3/2}$ photoelectrons through the alumina support, and were determined from the Tanuma et al. [26] algorithm, by using the QUASES-IMFP-TPP2M software [28].

In case of crystallite growth, the Ru particle size (c) can be estimated from the experimental value of XPS (Ru/Al) atomic ratio, by the following equation:

$$\frac{(Ru/Al)_{\text{exp}}}{(Ru/Al)_m} = \frac{1-e^{-c/\lambda_{Ru-Ru}}}{c/\lambda_{Ru-Ru}} \quad (8)$$

3. Results

3.1. Catalytic performance of Ru-supported nanoparticles

Results are shown in Table 1. Ammonia is produced with a selectivity of 100% over all the supported Ru catalysts. The highest nitrogen conversion and turnover frequency (TOF) are obtained for the Ru7/Al-WI catalyst, synthesized by wet impregnation with the highest Ru content. Among the catalysts containing 3 wt.% of Ru,

Table 1
Forward reaction rates and turnover frequencies (TOF) of ammonia synthesis performed over supported Ru catalysts. Conditions: N_2/H_2 = 1/3 vol.%, SV = 6000 ml/h/g_{cat}, 100 °C, 4 bar. Results obtained after 1 h.

Catalyst	% N_2 conversion	Forward reaction rate (μmol/g_{cat}/s)	TOF ($\times 10^{-2}$ s^{-1})
Ru7/Al-WI	9.4	1.75	2.50
Ru3/Al-WI	3.6	0.67	1.62
Ru7/Al-COLL	8.2	1.53	2.12
Ru3/Al-COLL	5.1	0.95	1.83
Ru2/Al-COLL	3.4	0.63	1.47
Ru3/Al-MIC BRIJ/heptane	1.7	0.32	0.44
Ru3/Al-MIC AOT/heptane	1.9	0.35	0.46
Ru3/Al-MIC CTAB/butanol	2.4	0.45	0.48
Ru3/Al-MIC CTAB/cycloehexane	3.2	0.59	0.48

the Ru3/Al-COLL catalyst presents the highest TOF value. In general, the best catalytic performances are obtained for the WI and COLL catalysts. For the catalysts prepared by microemulsion, the TOF value is very low and does not change when using different oil phases and solvents in the synthesis of the catalysts.

When comparing catalysts prepared by the same method (WI or COLL methods), an increase of the activity with the Ru loading is observed, both in terms of conversion and TOF.

3.2. Physicochemical characterization of the tested catalyst

Similar BET specific surface areas were measured for the catalysts synthesized by different methods and with different Ru loadings (Table A1).

In Table 2 are presented both the experimentally obtained XPS (Ru/Al) atomic ratios and the theoretical $(Ru/Al)_m$ ratios, calculated for a monolayer dispersion of ruthenium over the support (according to the model of Kerkhof et al. [24]). The percentage of the experimental atomic ratio, relative to the theoretical one, was also included as % of monolayer dispersion.

For WI and COLL catalysts, the percentage of monolayer dispersion is significantly low, meaning a low dispersion of the ruthenium on the γ-Al_2O_3 surface. For instance, only 26% of the monolayer dispersion is obtained for the Ru7/Al-WI catalyst. The MIC method leads to higher Ru dispersions (up to 66% of the monolayer dispersion, for the Ru3/Al-MIC CTAB/cycloehexane catalyst). The percentages of monolayer dispersion correspond to the XPS $(Ru/Al)_{exp}$ atomic ratio.

For catalysts prepared by WI and COLL methods, the percentage of Ru monolayer dispersion decreases with the Ru loading, indicating that lower amounts of ruthenium are well dispersed over alumina. Accordingly, for catalysts prepared by the same method, the Ru particle size increases with the content of Ru. All catalysts prepared by the MIC method present smaller Ru nanoparticles, whose sizes change slightly for different oil phases and a constant Ru loading.

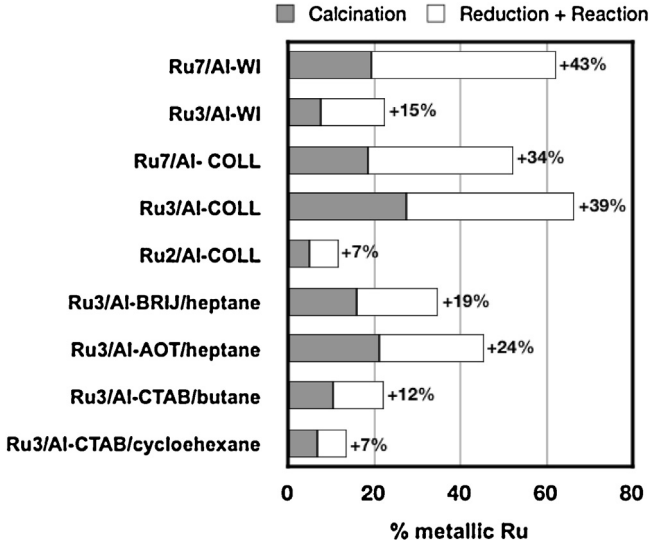

Fig. 1. XPS Ru^0 atomic concentration in calcined (gray bar) and tested (gray and white bars) catalysts.

Because of the presence of very small nanoparticles in most catalysts, the X-ray analysis does not give a reliable estimation of the particle sizes (Fig. A1).

The decomposition of XPS Ru3d peaks into 3 characteristic doublets at 279.9, 281.0 and 282.5 eV can be associated with the presence of Ru^0, RuO_2 and RuO_3 species, respectively [29–31], as shown in Fig. A2 for the Ru7/Al-WI tested catalyst. The surface proportions of those species were quantified in order to analyze the changes of Ru oxidation state during the reaction over different catalytic surface configurations.

Note that the XPS analysis was not performed in situ. Indeed, after the catalytic test, the sample was cooled down to room temperature under inert gas flow, so that any possible oxidation of the catalyst by exposure to air, during its transfer into the XPS machine, is expected to be minor and would only concern the most external surface layer. Furthermore, the XPS analysis may involve a mild reduction associated with the exposure to ultra-high vacuum conditions (10^{-5} Torr) [32]. Then, if some oxidized ruthenium species were formed in the outer layer while under air, they would be re-reduced at this stage.

The percentage of surface Ru atoms present as Ru^0 after the catalyst calcination is shown in Fig. 1 (gray bar) along with the percentage of Ru^0 atoms reached after the reduction step and the subsequent reaction (white bar).

Table 2
XPS analysis of Ru dispersion over γ-Al_2O_3, for catalysts tested at 100 °C and 4 bar.

Catalyst	XPS (Ru/Al) atomic ratio		% of Ru monolayer dispersion	Average particle size[a] (nm)
	$(Ru/Al)_m$	$(Ru/Al)_{exp}$		
Ru7/Al-WI	0.092	0.024	26	6.1
Ru3/Al-WI	0.038	0.013	34	4.4
Ru7/Al-COLL	0.092	0.025	27	5.9
Ru3/Al-COLL	0.038	0.014	37	4.1
Ru2/Al-COLL	0.025	0.011	44	3.1
Ru3/Al-MIC BRIJ/heptane	0.038	0.019	50	2.6
Ru3/Al-MIC AOT/heptane	0.038	0.020	53	2.4
Ru3/Al-MIC CTAB/butanol	0.038	0.022	58	2.0
Ru3/Al-MIC CTAB/cycloehexane	0.038	0.025	66	1.5

[a] Sizes estimated according to the model of Kerkhof et al. [24].

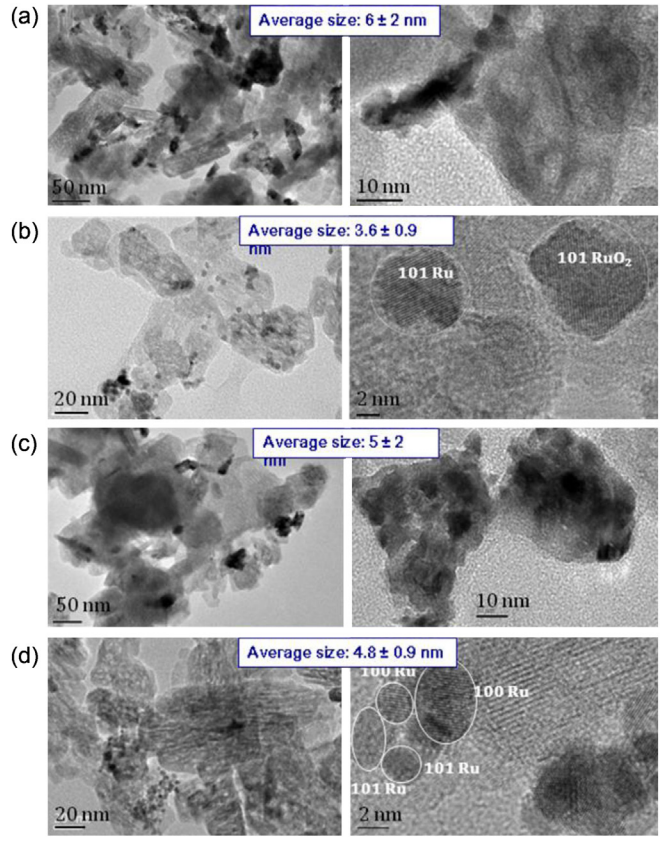

Fig. 2. TEM images of Ru nanoparticles supported on γ-Al_2O_3 for (a) Ru7/Al-WI, (b) Ru7/Al-COLL, (c) Ru3/Al-WI and (d) Ru3/Al-COLL. All catalysts tested at 100 °C and 4 bar.

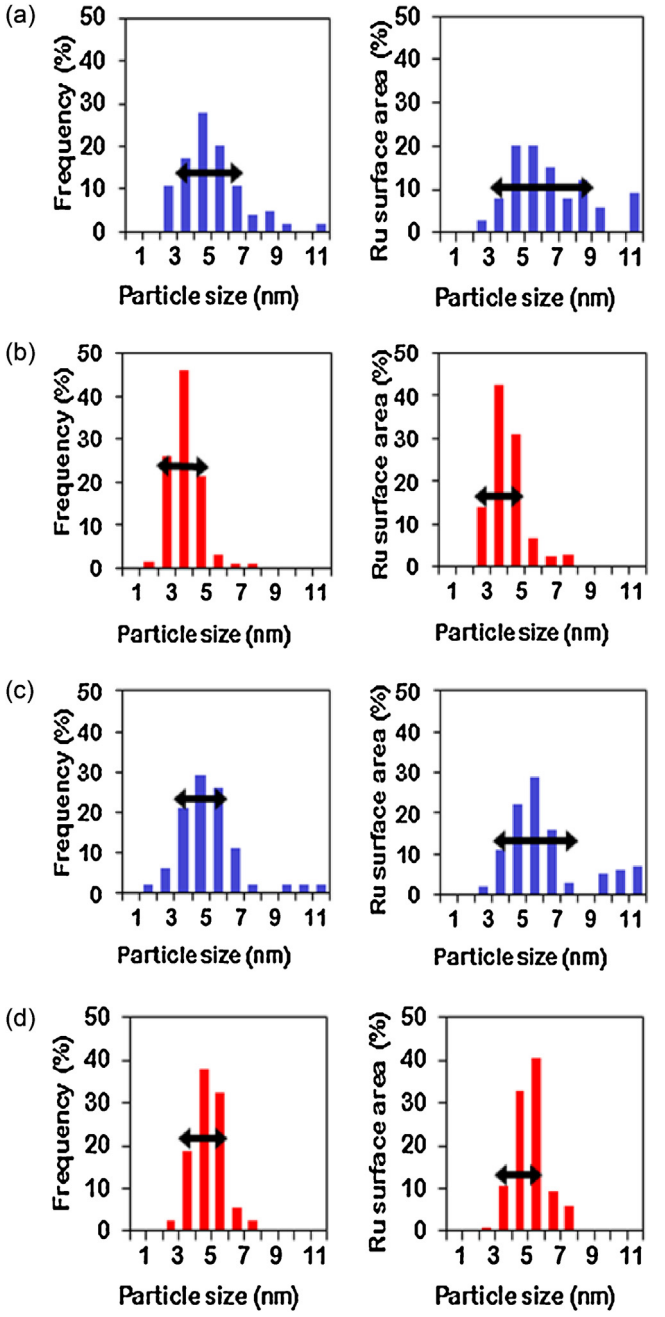

Fig. 3. Histograms of frequency and Ru surface area, corresponding to the Ru nanoparticles measured by TEM in (a) Ru7/Al-WI, (b) Ru7/Al-COLL, (c) Ru3/Al-WI and (d) Ru3/Al-COLL. The black arrows showing both 80% of cumulative frequency and 80% of total Ru surface area.

The surface concentration of remaining Ru^0 after calcination ranges from 5 to 30%. During the reduction and the reaction, this concentration increases in about 100% for the MIC catalysts, 150% for the COLL catalysts, and 200% for the WI catalysts. Among catalysts prepared by the same method, higher Ru contents lead to higher reduction of Ru surface atoms during the reduction and the reaction. The highest percentage of Ru reduced into Ru^0 during the reduction and the reaction is observed for the Ru7/Al-WI, Ru7/Al-COLL and Ru3/Al-COLL catalysts (43%, 34% and 39%, respectively). For Ru3/Al-WI, only 15% of Ru^0 is formed during the reduction and the reaction. For the catalysts prepared by microemulsion (MIC), the concentration of Ru^0 reached after the reaction is lower than for Ru7/Al-WI, Ru7/Al-COLL and Ru3/Al-COLL. In addition, the percentage of Ru^0 formed during the reduction the reaction is also lower for MIC catalysts (5–15%).

The TEM analysis evidences significant differences in the surface configuration, dispersion, size distribution and crystallinity of Ru supported particles. In Fig. 2, some TEM pictures of tested WI and COLL catalysts are presented along with the average size and standard deviation. In most cases, the mean sizes of Ru nanoparticles are reasonably in good agreement with the values estimated from the XPS (Ru/Al) atomic ratios (Table 2). The latter has been used to calculate the TOF values and will be the size values considered in the discussion (Section 4).

The WI method leads to the formation of barely visible Ru nanoparticles, presenting a highly broad distribution of particle sizes (standard deviation of 2 nm). Most of them are forming large agglomerates, although few isolated particles are also observed. This is clearly shown by the TEM images of tested Ru7/Al-WI and Ru3/Al-WI catalysts, presented in Fig. 2a and c. The average size of Ru nanoparticles is 6 nm (±2 nm) for Ru7/Al-WI and 5 nm (±2 nm) for Ru3/Al-WI.

The samples prepared by the COLL method contain well-defined round Ru nanoparticles with a narrower size distribution (standard deviation of 1 nm). As observed in the TEM images of tested Ru3/Al-COLL and Ru7/Al-COLL catalysts, the particles are well separated and do not form the large clusters observed in WI catalysts. The Ru7/Al-COLL catalyst (Fig. 2b) presents Ru nanoparticles with a mean size of 3.6 nm (±0.9 nm), whereas the average Ru particle size in the Ru3/Al-COLL catalyst (Fig. 2d) is 4.8 nm (±0.9 nm).

A way to fully grasp the size distribution is to plot the frequency histogram in terms of contribution to the total Ru surface area (see Fig. 3). The large Ru nanoparticles indeed present a higher surface

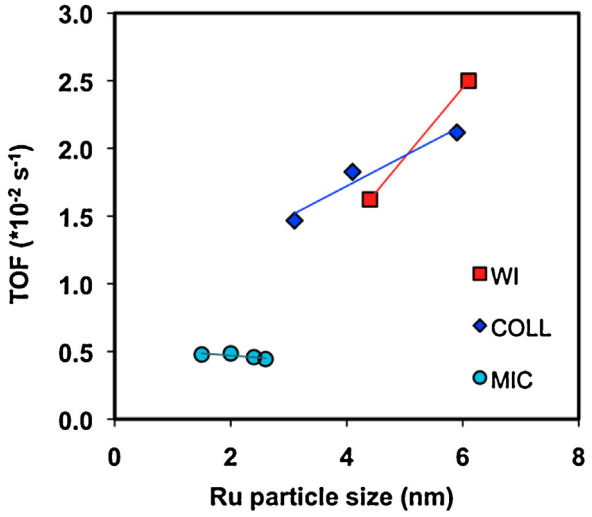

Fig. 4. TOF as a function of the average size of Ru nanoparticles.

than the smaller ones. As a consequence, describing 80% of particles is not necessarily equivalent to describing 80% of Ru surface area. As the size distribution is very narrow for the COLL catalysts, the range of concerned particles (80%) does not evolve when considering the percentage of Ru surface area instead of the frequency of particles. It is, in both cases, (2–5 nm) for Ru7/Al-COLL and (3–6 nm) for Ru3/Al-COLL. However, this range increases for the WI catalysts, mostly for Ru7/Al-WI: from (3–7 nm) to (3–9 nm) for Ru7/Al-WI and from (3–6 nm) to (3–8 nm) for Ru3/Al-WI. Looking at those histograms, Ru7/Al-WI appears as the only sample where a significant part of the Ru surface area corresponds to particles between 7 and 9 nm.

High resolution TEM apparatus was used to measure and identify the Ru crystalline planes in some tested catalysts (Fig. 2b and d). Among the planes detected, the most part corresponds to (1 0 1) and (1 0 0) planes of hexagonal Ru^0 (2.06 Å and 2.34 Å), although some (1 1 0) and (1 0 1) planes of tetragonal RuO_2 (3.18 Å and 2.56 Å) were also measured. Given the small size and roundness of the Ru particles, many steps and edges exist, independently of the exposed planes and the particle orientation. Therefore, many sites similar to the B_5-type active ones could be expected to be present.

4. Discussion

4.1. Effect of the size of ruthenium nanoparticles on the catalytic activity

An increase of the TOF values with the Ru loading was observed for the catalysts prepared by WI and COLL methods (Table 1). It was also shown that higher contents of Ru lead to higher average sizes of Ru nanoparticles, when the same synthesis method is used (Table 2). It can be concluded that the TOF in ammonia synthesis increases with the Ru particle size (for mean sizes up to 6 nm), which means that Ru active sites are present in greater amounts over larger nanoparticles. This is clearly illustrated in Fig. 4: Ru7/Al-WI is the most active catalyst (TOF = 2.5×10^{-2} s^{-1}) having the highest average Ru particle size (6.1 nm), whereas all MIC catalysts present a very low activity (TOF = 0.44–0.48 $\times 10^{-2}$ s^{-1}) and the smallest particle sizes (1.5–2.6 nm). For the COLL catalysts, the TOF value increases almost linearly with the size of the Ru particle.

However, the different mean sizes of Ru nanoparticles do not fully explain the differences in catalytic activity. In Fig. 4 there are cases in which different TOF values are obtained for catalysts having very similar average size of Ru nanoparticles. The Ru7/Al-WI catalyst is 18% more active than Ru7/Al-COLL, both presenting

Table 3
Statistical description of the catalysts analyzed by TEM: (a) Ru nanoparticles constituting 80% of the cumulative frequency and 80% of the total Ru surface area; (b) Ru nanoparticles in the (7–9 nm) range.

(a)

Catalyst	80% of cumulative frequency			80% of total Ru surface area		
	Exact %	Range (nm)	Δ size (nm)	Exact %	Range (nm)	Δ size (nm)
Ru7/Al-WI	76	3–7	3	83	3–9	5
Ru7/Al-COLL	93	2–5	2	87	2–5	2
Ru3/Al-WI	76	3–6	2	81	3–8	4
Ru3/Al-COLL	89	3–6	2	84	3–6	2

(b)

Catalyst	Particles in the (7–9 nm) range	
	Frequency (%)	Ru surface area (%)
Ru7/Al-WI	9	20
Ru7/Al-COLL	1	3
Ru3/Al-WI	2	3
Ru3/Al-COLL	3	6

Ru nanoparticles with an average size of 6 nm. Similarly, Ru3/Al-COLL catalyst is 13% more active than Ru3/Al-WI, even though the average particle size of the latter is slightly higher (4.1 nm and 4.4 nm, respectively). An even greater difference in the TOF is observed between the Ru2/Al-COLL catalyst and the Ru3/Al-MIC BRIJ/heptane catalyst, with similar average size of Ru nanoparticles.

This suggests that, besides the size of Ru nanoparticles, the synthesis method affects the surface configuration, which has an important effect on the catalytic performance. A better understanding of the surface configuration and how it affects the catalytic performance is accomplished by analyzing the TEM images, as shown in next section.

4.2. Implications of ruthenium particle size distribution and surface configuration on the catalytic activity

A careful comparison between the TEM images of the Ru7/Al-WI catalyst and Ru7/Al-COLL has been done to explain the higher activity (TOF difference of 18%) of Ru7/Al-WI despite having similar average sizes of Ru nanoparticles. Indeed, both catalysts contain Ru nanoparticles with a mean size of about 6 nm and the same dispersion over the surface, according to XPS results (i.e., the same XPS (Ru/Al) atomic ratio). But TEM analysis reveals significant differences in the surface configuration of both samples. The WI catalyst present more agglomerated Ru nanoparticles with a broader size distribution (standard deviation of 2 nm, against 1 nm for the COLL catalyst). This means that to achieve a high catalytic activity not only a high average size of Ru nanoparticles is required, but also a broad size distribution, including proximity of both small and large nanoparticles.

However, the broadness of the size distribution cannot fully explain the catalytic results for the samples containing 3 wt.% of ruthenium. Ru3/Al-COLL is 13% more active than Ru3/Al-WI, although both catalysts present Ru nanoparticles with similar mean sizes (4.1 and 4.4 nm) and the size distribution is still broader for the WI catalyst (±2 nm, against ± 1 nm for the Ru3/Al-COLL). Besides the standard deviation argument, these two samples differ in the Ru surface area developed from the particles in the (7–9 nm) range (see Table 3a and b). The fraction of Ru surface corresponding to the (7–9 nm) particles is considerably lower for Ru3/Al-WI than for Ru3/Al-COLL, which suggests that the lack of these large nanoparticles in the Ru3/Al-WI sample could cause its lower activity. Moreover, the higher TOF value of Ru7/Al-WI (about 60% higher)

compared with Ru3/Al-WI, could also be a contribution of the lower amount of (7–9 nm) Ru nanoparticles in the latter catalyst. It is important to note that some preliminary catalytic tests have been performed, under mild reaction conditions, over catalysts containing Ru nanoparticles with mean sizes higher than 10 nm. Low activities were obtained compared to those presented for the highest mean sizes analyzed in this article. This indicates that while large Ru nanoparticles in the (7–9 nm) range were found to contribute significantly to higher activities, the presence of even larger particles could be detrimental to the catalytic performance.

The importance of the presence of small Ru nanoparticles for a high catalytic performance in ammonia synthesis has been already reported in literature. Theoretical calculations have shown that the concentration of B_5-type sites, being the most active, is high on small crystals (2 nm) of supported ruthenium, and decline for smaller and larger particles size [13–15]. Additionally, catalytic tests under conditions of high temperature (200–500 °C) and pressure (100 bar) have confirmed this 2 nm optimum size [15].

Small (around 2.6 nm) and very small (<2 nm) Ru nanoparticles have indeed been obtained for the catalysts prepared by microemulsion. A low activity (TOF $\sim 0.5 \times 10^{-2}$ s^{-1}) was obtained in all cases. It is noteworthy that the activity of the Ru2/Al-COLL catalyst is about 3 times the activity of the Ru3/Al-MIC BRIJ/heptane catalyst, even though they present a similar average size of Ru nanoparticles. This difference may be attributed to Ru surface pollution associated with the synthesis by microemulsion, more than to the broader size distribution of Ru nanoparticles in Ru2/Al-COLL.

It can be concluded that a high catalytic performance in ammonia synthesis can be achieved by Ru supported nanoparticles having a relatively high mean size and a broad size distribution that would ensure the presence of small nanoparticles (~2 nm) and also larger particles with a probable optimal size of 7–9 nm. This is for the first time issued for ammonia synthesis and it could be a characteristic aspect of the process operating under mild operational conditions (100 °C and 4 bar).

4.3. Catalytic cooperation between small and large nanoparticles

It has been shown that the catalytic activity increases in presence of large (7–9 nm) Ru nanoparticles, even though the most active sites (B_5-type sites) are preferentially formed on small particles [13,15]. Additionally, the most active catalyst (Ru7/Al-WI) presents the highest concentration of both small and large Ru nanoparticles forming part of big clusters, which allows a high number of contacts between the particles. This suggests that, under mild reaction conditions, a catalytic cooperation may occur between the small and large Ru particles, when they are in good contact.

In order to verify the existence of such a cooperative effect, mixtures of Ru7/Al-WI (containing a high concentration of both small and large Ru nanoparticles, mean size 6.1 nm) and Ru3/Al-WI (still broad size distribution, mean size 4.4 nm) were prepared by mechanically mixing both catalysts in different percentages, which is expected to result in a close contact between particles of different sizes. If this contact has no effect on the activity, the expected TOF values of the mixture would correspond to the weighted average of the TOF values obtained for each component, as single catalysts. The results of the catalytic tests are presented in Fig. 5, where the straight line represents the theoretical values (in absence of a cooperative effect). An important synergistic effect is observed for the mechanical mixtures with high Ru7/Al-WI contents, and the effect is maximum for the mixture containing 50 wt.% of Ru7/Al-WI. For this sample, the XPS $(Ru/Al)_{exp}$ atomic ratio corresponds to the addition of the values for the single catalysts composing the mixture (Table 4), indicating that there is no enrichment of the surface in ruthenium atoms as a consequence

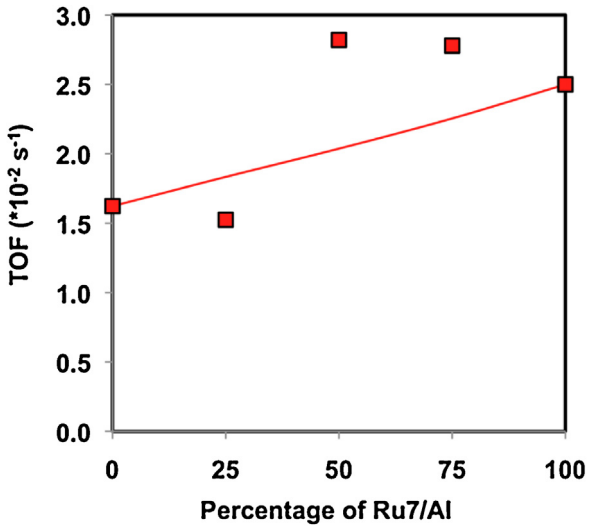

Fig. 5. TOF as a function of Ru7/Al-WI content in the mechanical mixtures. The straight line corresponding to the weighted average values of the TOF obtained for the single Ru3/Al-WI and Ru7/Al-WI catalysts.

of the mixing procedure and the catalytic test. Therefore, the synergistic effect can be explained as a cooperative effect between small and large Ru-supported nanoparticles, when they are in good contact.

4.4. Proposal of a catalytic mechanism for ammonia synthesis over Ru supported nanoparticles operating at mild conditions

According to the XPS quantification of the Ru^0 concentration at the catalyst surface (presented in Fig. 1), the most active catalysts (Ru7/Al-WI, Ru7/Al-COLL and Ru3/Al-COLL) undergo further reduction of Ru surface atoms during the reduction and the reaction. The highest percentage of reduction (43%) was obtained for the Ru7/Al-WI catalyst, which presents Ru particles with a mean size of 6.1 nm and the broadest size distribution, including large nanoparticles. This indicates that a highly reduced Ru surface is required for a high activity and that the presence of large Ru nanoparticles may promote the reduction of ruthenium during the catalytic test.

A cooperative effect between small and large nanoparticles on the reduction of Ru surface, under reaction conditions, is clearly shown in Table 4 for the 50Ru3/Al-WI + 50Ru7/Al-WI mixture having the highest activity. The concentration of surface (XPS) metallic Ru reached during the reduction and the reaction is 67% higher than the average value corresponding to the reduction of single catalysts (42%). However, according to the temperature programmed reduction (TPR) analysis of 50Ru3/Al-WI + 50Ru7/Al-WI and the single catalysts forming part of the mixture (Fig. 6), there is no synergy in the bulk reduction of ruthenium. This suggests that the cooperative effect occurs at the Ru surface under reaction conditions (in presence of both nitrogen and hydrogen reactive gases). It can be

Table 4
XPS analysis for 50Ru3/Al-WI + 50Ru7/Al-WI and the single catalysts composing the mixture, all tested at 100 °C and 4 bar.

Catalyst	XPS $(Ru/Al)_{exp}$ atomic ratio	Average particle size[a] (nm)	XPS Ru^0 atomic concentration (%)
Ru7/Al-WI	0.024	6.1	62.3
50Ru3/Al-WI + 50Ru7/Al-WI	0.019	5.4	70.7
Ru3/Al-WI	0.013	4.4	22.5

[a] Sizes estimated according to the model of Kerkhof et al. [24].

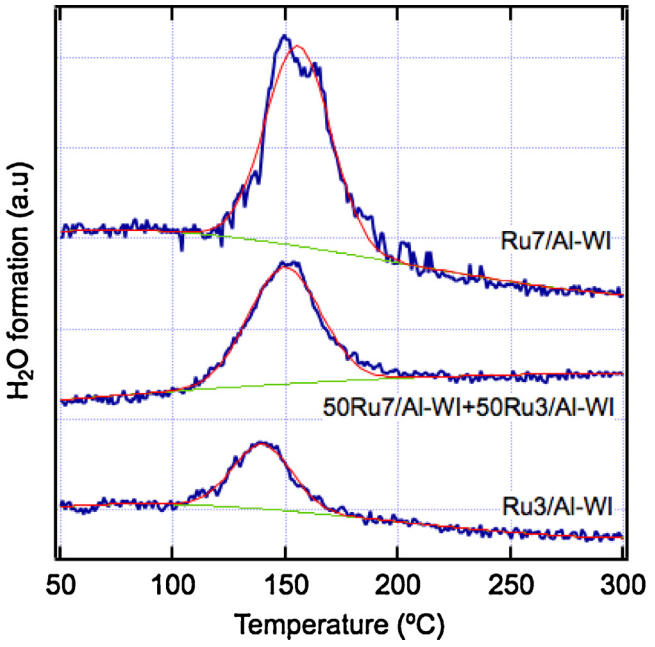

Fig. 6. TPR profiles obtained for Ru3/Al-WI, Ru7/Al-WI and 50Ru3/Al-WI + 50Ru7/Al-WI catalysts.

concluded that the same cooperation between small and larger Ru nanoparticles leads to the promotion of surface Ru reduction and the synergistic effect in the catalytic activity.

It has been reported that nitrogen is strongly adsorbed and hardly hydrogenated over very small Ru particles (<2 nm), having a reduced number of B_5-type sites [13]. This affects the NH_3 synthesis rate by decreasing the number of active sites for the dissociative adsorption of N_2, which corresponds to the rate-determining step. During the reaction, the amount of adsorbed nitrogen increases and starts blocking the surface, whereas the fraction of hydrogen adsorbed decreases. This is consistent with the low activity obtained for the catalysts prepared by microemulsion, containing very small Ru nanoparticles with a narrow size distribution.

The B_5 sites have been found to reach an optimum level over slightly larger particles (~2 nm), where crystallographic planes can be formed. It is noteworthy that these results were obtained, by theoretical calculations, from model-nanoparticles exposing only their 001 and 100 faces with an isotropic hexagonal shape, and therefore all the B_5 sites present part of their atoms on a crystal edge. Our catalysts mostly present spherical-shaped Ru particles, with mean sizes between 4 and 6 nm, meaning numerous Ru atoms on edges. This suggests that in our case, the optimum level of B_5 sites may be obtained for particles slightly larger than 2 nm, probably in the range 7–9 nm.

Besides the presence of B_5 sites in the (7–9 nm) particles, a supplementary argument is required to understand the importance of a broad size distribution for a high catalytic activity and the synergic effect between small and larger particles. It could be admitted that in large nanoparticles there is a high concentration of ruthenium atoms on terraces, which exhibit low activity for N_2 dissociation. We propose that large nanoparticles promote the reaction rate of ammonia synthesis, by providing sites for the hydrogen activation. When a good contact exists between the particles, the hydrogen atoms (H^*) activated in large particles may migrate along the surface, reaching the strongly adsorbed nitrogen atoms in small particles or flat surfaces. The hydrogenation of these nitrogen atoms would allow releasing active sites for the dissociative adsorption of new N_2 molecules. The transfer of H^* atoms would also promote the activation of N_2 by keeping a high fraction of metallic Ru sites on the catalytic surface, as indicated by the XPS analysis.

The proposed catalytic mechanism would then explain the high catalytic performances of catalyst containing Ru particles with a broad size distribution, and the low activity obtained for narrow size distributions.

5. Conclusions

Catalysts with different average size and size distribution of Ru nanoparticles were studied in the ammonia synthesis under mild reaction conditions (100 °C, 4 bar) and characterized principally by XRD, XPS and HR-TEM techniques.

It was demonstrated that (i) the activity increases with the mean size of Ru nanoparticles in the range 2–10 nm; (ii) for similar average sized Ru particles, a narrow distribution of sizes leads to a lower activity; (iii) it is possible to benefit from synergic effect between large and small sized nanoparticles to obtain higher activities.

Large Ru nanoparticles promote the reaction under mild conditions (low temperature and pressure), even though the B_5-type sites (most active sites) are preferentially formed on small particles, which suggests that a catalytic cooperation may occur between the particles, when they are in near proximity. This cooperation was verified by preparing mechanical mixtures of two catalysts containing different sizes. An important synergy in the activity was obtained with the mixtures. It is suggested that large Ru nanoparticles promote the reaction rate by providing sites for the hydrogen activation. The activated hydrogen atoms may migrate along the surface, reaching the strongly adsorbed nitrogen in small particles. The hydrogenation of these nitrogen atoms would allow releasing active sites for the dissociative adsorption of new N_2 molecules, corresponding to the rate determining step of ammonia synthesis, thus increasing catalytic performances.

6. Outlook

In this work it is proposed that the synthesis of ruthenium-supported nanoparticles with controlled size allows performing the ammonia synthesis reaction at low temperature via a mechanism in which the Ru particle size and the broadness of the size distribution play a crucial role.

For Ru-supported catalyst, it was shown that the activity increases with the average size of Ru particles and that for similar range sized particles, a narrow distribution of sizes leads to lower activities and a heterogeneous distribution of sizes favors a higher activity. It is noteworthy that a similar effect of the nanoparticle size on the catalytic activity has been found for other catalytic processes operating at mild conditions (e.g. CO_2 hydrogenation over Rh-supported catalysts) [33,34]. This suggests that the catalytic cooperation between large and small nanoparticles may be generalized to other noble metals supported crystallites, catalyzing reactions in presence of hydrogen.

Acknowledgements

Financial support of the Belgium National Fund for Scientific Research (FSR-FNRS) and 'Becas Chile' program of CONICYT (Chile) are gratefully acknowledged. The authors also acknowledge the "Direction Générale des Technologies, de la Recherche et de l'Energie (DGTRE)" of the "Région Wallonne" (Belgium) and the "Fonds National de la Recherche Scientifique (FNRS)" of Belgium, and the involvement of IMCN-MOST in the "INANOMAT" IUAP network sustained by the "Service public fédéral de programmation politique scientifique" (Belgium). Cooperation between MOST and LCMCP has here been founded by the PHC (partenariat Hubert Curien) named Tournesol Program.

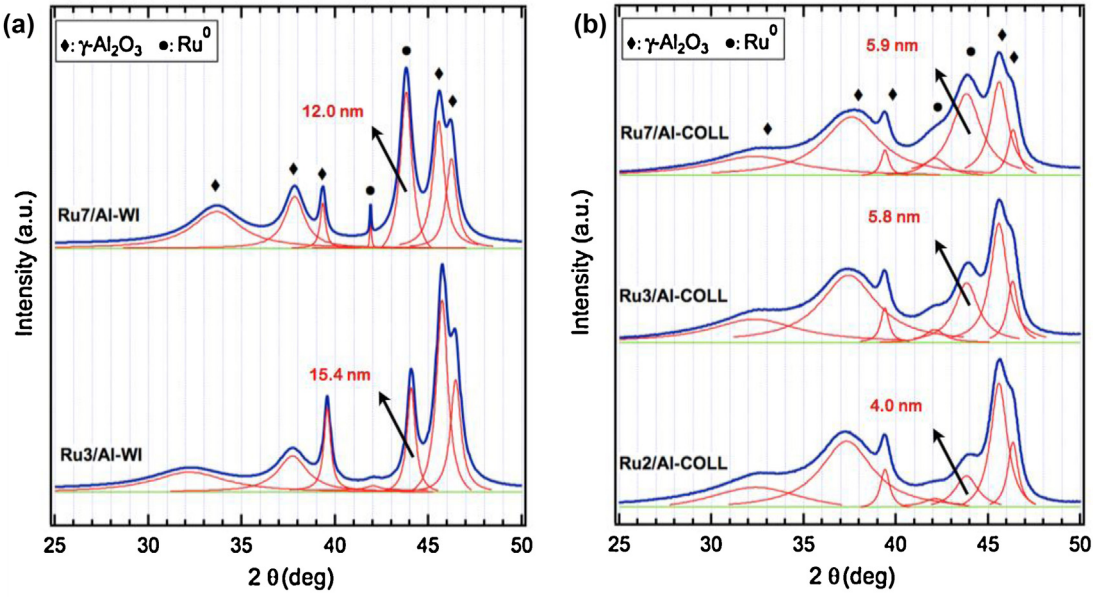

Fig. A1. XRD spectrum obtained of the (a) Ru/Al-WI and (b) Ru/Al-COLL tested catalysts.

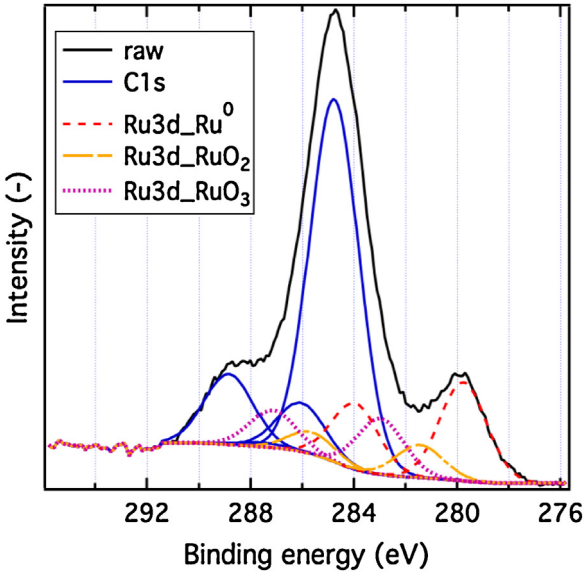

Fig. A2. Decomposition of the XPS C1s peak of the Ru7/Al-WI tested catalyst.

Appendix A.

Figs. A1 and A2.
Table A1.

Table A1
BET specific surface area of the catalysts prepared by wet impregnation, colloidal and microemeulsion methods, calcined at 450 °C.

Catalyst	Ru (wt.%)	S_{BET} (m^2/g)
γ-Al_2O_3	–	73
Ru7/Al-WI	7	68
Ru3/Al-WI	3	70
Ru7/Al-COLL	7	75
Ru3/Al-COLL	3	65
Ru2/Al-COLL	2	71
Ru3/Al-MIC BRIJ/heptane	3	79
Ru3/Al-MIC AOT/heptane	3	68
Ru3/Al-MIC CTAB/butanol	3	65
Ru3/Al-MIC CTAB/cycloehexane	3	69

References

[1] T.H. Rod, A. Logadottir, J.K. Nørskov, J. Chem. Phys. 112 (2000) 5343.
[2] V.B. Shur, S.M. Yunusov, Russ. Chem. Bull. 47 (1998) 765–776.
[3] K. Aika, H. Hori, A. Ozaki, J. Catal. 27 (1972) 424.
[4] K. Aika, A. Ohya, A. Ozaki, Y. Inoue, I. Yasumori, J. Catal. 92 (1985) 305.
[5] O. Hinrichsen, F. Rosowski, A. Hornung, M. Muhler, G. Ertl, J. Catal. 165 (1997) 33–44.
[6] A. Miyazaki, I. Balint, K. Aika, Y. Nakano, J. Catal. 204 (2001) 364–371.
[7] S. Wu, J. Chen, X. Zheng, H. Zeng, C. Zheng, N. Guan, Chem. Commun. 248 (2003) 8–2489.
[8] P. Seetharamulu, V.S. Kumar, A.H. Padmasri, B.D. Raju, K.S.R. Rao, J. Mol. Catal. A: Chem. 263 (2007) 253–258.
[9] C. Burda, X. Chen, R. Narayanan, M. El-Sayed, Chem. Rev. 105 (2005) 1025.
[10] C. Harding, V. Habibpour, S. Kunz, A. Nam-Su Farnbacher, U. Heiz, B. Yoon, U. Landman, J. Am. Chem. Soc. 131 (2009) 538.
[11] A. Logadottir, T.H. Rod, J.K. Nørskov, B. Hammer, S. Dahl, C.J.H. Jacobsen, J. Catal. 197 (2001) 229–231.
[12] J.K. Nørskov, T. Bligaard, A. Logadottir, S. Bahn, L.B. Hansen, M. Bollinger, H. Bengaard, B. Hammer, Z. Sljivancanin, M. Mavrikakis, Y. Xu, S. Dahl, C.J.H. Jacobsen, J. Catal. 209 (2002) 275–278.
[13] S. Dahl, A. Logadottir, R.C. Egeberg, J.H. Larsen, I. Chorkendorff, E. Törnqvist, J.K. Nørskov, Phys. Rev. Lett. 83 (9) (1999) 1814–1817.
[14] S. Dahl, J. Sehested, C.J.H. Jacobsen, E. Törnqvist, I. Chorkendorff, J. Catal. 192 (2000) 391–399.
[15] C.J.H. Jacobsen, Søren Dahl, Poul L. Hansen, Eric Törnqvist, Lone Jensen, Henrik Topsøe, Dorthe V. Prip, Pernille B. Møenshaug, I. Chorkendorff, J. Mol. Catal. A 163 (2000) 19–26.
[16] B. Lin, K. Wei, J. Lin, J. Ni, Catal. Commun. 39 (2013) 14–19.
[17] Z. Kowalczyk, S. Jodzis, W. Rarog, J. Zielinski, J. Pielaszek, A. Presz, Appl. Catal. A 184 (1999) 95–102.
[18] W. Raróg-Pilecka, E. Miskiewicz, D. Szmigiel, Z. Kowalczyk, J. Catal. 231 (2005) 11–19.
[19] C.H. Liang, Z.B. Wei, Q. Xin, C. Li, Appl. Catal. A 208 (2001) 193–201.
[20] C. Sassoye, G. Muller, D.P. Debecker, A. Karelovic, S. Cassaignon, C. Pizarro, P. Ruiz, C. Sanchez, Green Chem. 13 (2011) 3230–3237.
[21] S. Eriksson, U. Nylén, S. Rojas, M. Boutonnet, Appl. Catal. A 265 (2004) 207–219.
[22] X. Zhang, K.Y. Chan, Chem. Mater. 15 (2003) 451–459.
[23] Y. Li, C.W. Park, Langmuir 15 (1999) 952–956.
[24] F.P.J.M. Kerkhof, J.A. Moulijn, J. Phys. Chem. 83 (1979) 1612–1619.
[25] T. Talonen, J. Eskelinen, T. Syvajarvi, A. Roine, Outokumpu HSC Chemistry for Windows, 4.0 ed., 1999.
[26] S. Tanuma, C.J. Powell, D.R. Penn, Surf. Interface Anal. 21 (1994) 165–176.
[27] J.H. Scofield, J. Electron Spectrosc. 8 (1976) 129–137.
[28] S. Tougaard, QUASES-IMFP-TPP2M Software, Quases-Tougaard Inc., Denmark, 2002.
[29] C. Elmasides, D.I. Kondarides, W. Gru1nert, X.E. Verykios, J. Phys. Chem. B 103 (1999) 5227–5239.
[30] Y.V. Larichev, L. Boris, Moroz, I. Valerii, Bukhtiyarov, Appl. Surf. Sci. 258 (2011) 1541–1550.
[31] J. Okal, M. Zawadzki, W. Tylus, Appl. Catal. B 101 (2011) 548–559.
[32] P. Froment, M.J. Genet, M. Devillers, J. Electron Spectrosc. Relat. Phenom. 104 (1999) 119–126.
[33] A. Karelovic, P. Ruiz, Appl. Catal. B 113–114 (2012) 237–249.
[34] A. Karelovic, P. Ruiz, J. Catal. 301 (2013) 141–153.